
Check for updates

were interpreted w
calculations to clarify the
SnO_4 pyramids with the lone-pair
structural units obtained. In the search for gl
response, several interesting property changes were de
SnO-ZnO-P_2O_5 system [10]. These results gave rise to structural investigations including diffraction [18]. The combined analysis of neutron and X-ray diffraction (XRD) results allowed the determination of Sn−O bonds with lengths up to 0.26 nm, and these analyses revealed a clear change from SnO_3 to SnO_4 units when ZnO replaced SnO in a series of glasses with 33.3 mol% P_2O_5. SnO_3 pyramids were found for the binary 66.7SnO-33.3P_2O_5 glass.

The present work reports results of diffraction experiments on binary $(SnO)_x(P_2O_5)_{1-x}$ glasses with $0.5 \le x \le 0.7$, using diffraction experiments similar to those performed on the Sn/Zn-pyrophosphate glasses [18]. XRD measurements of the present study were made with 115 keV photons instead of 60 keV photons [18] which yields a larger range for the scattering vector.

2. Experimental

2.1. Samples

Sample preparation and glass properties are described in [7]. Ten gram mixtures of reagent grade SnO, $Sn_2P_2O_7$, and P_2O_5 were melted for 15 min at 1000 °C in carbon crucibles in a silica tube furnace under flowing dry argon to avoid oxidation of Sn^{2+}. The homogeneous melts were quenched on copper plates in air. Five samples of $(SnO)_x(P_2O_5)_{1-x}$ glasses with $x = 0.50$, 0.55, 0.60, 0.67 and 0.70 were used in the measurements. The samples are labelled SNPxx with xx indicating the SnO content in mole%. As described in [7], the water contents of these glasses decreased with increasing SnO-contents, but were all under 1500 ppm. There was no evidence for the presence of Sn^{4+} in any sample, and nominal compositions were assumed from minimal weight losses during processing.

2.2. X-ray diffraction

The XRD experiments were performed at the BW5 wiggler beamline of the synchrotron DORIS III (Deutsches Elektronen-Synchrotron DESY Hamburg). The incident photon energy was 114.5 keV, i.e. the radiation wavelength λ was 0.01083 nm. The glassy powders were loaded into thin-walled silica capillaries (2 mm diameter) and exposed to the beam by a slit 1x4 mm^2. The scattering intensities were obtained in a step-scan mode using a solid-state Ge-detector that was moved horizontally on a straight sliding carriage. The decay of the intensity of the primary beam during the synchrotron run was monitored by a diode detector. The intensities were obtained in two or three runs in intervals of scattering angle 2θ (0.5°-16°, 15°-28°, 21°-28°) with an absorber to reduce the effects of the detector dead-time in the first interval and a widened detector slit in the third interval. The scattering data were corrected for dead-time, background, container scattering, polarization, absorption, and a varying sample-detector distance. The merged experimental scattering intensities were normalized to the structure-independent X-ray scattering functions which were calculated in accordance with the chemical composition of each sample. This scattering is the weighted sum of a polynomial approach of the tabulated atomic factors of elastic scattering and the Compton scattering [19–21]. Subsequently, the calculated Compton fraction was removed and the total Faber-Ziman structure factor $S_X(Q)$ was obtained from the normalized scattering intensity [22,23]. Q is the magnitude of momentum transfer of elastic scattering with $Q = (4\pi/\lambda)\sin\theta$. The scattering data of a few detector runs showed unphysical features due to beam instabilities as they can occur after synchrotron injection. Such data were discarded. Therefore, the structure factors show different degrees of noise at large Q-values.

Serious normalization problems occurred in the vicinity of
mismatch in the results. As a result, the common normalization was performed only for $Q < 180\,nm^{-1}$ and smooth functions were introduced for $Q > 180\,nm^{-1}$ around which the experimental curves were forced to oscillate.

2.3. Neutron diffraction

The neutron diffraction experiments were performed at the GEM instrument of the spallation source ISIS of the Rutherford Appleton Laboratory (Chilton/ UK). The powdered sample material was loaded into thin-walled vanadium cylinders (diameter, 10.3 mm). The duration of data acquisition was at least five hours per sample. A vanadium rod (diameter, 9.8 mm) was used to determine the incident energy spectrum which was needed for the data normalization in the time-of-flight regime. The data were corrected using standard procedures for container and background scattering, attenuation, multiple scattering and inelasticity effects [25]. The differential scattering cross-sections of the detector groups 2, 3, 4, and 5 (scattering angles 14°-109°) were normalized to the calculated mean scattering that was calculated from the tabulated neutron scattering lengths. Finally, neutron Faber-Ziman structure factors, $S_N(Q)$ were obtained [22,23].

3. Results

The corrected and normalized neutron and X-ray diffraction results of the tin phosphate glasses are shown in Fig. 1 by means of the interference functions which are weighted by factor Q. The experimental data are compared with model curves, which are composed of damped sinusoidal functions. The latter curves were calculated with the parameters of those Gaussian functions that were used to fit the first peaks in the real-space correlation functions, $T(r)$. Fig. 1 shows good agreement between the model and experimental data for $Q > 50\,nm^{-1}$, the scattering range of the short-range order. The amplitudes of the oscillations in the scattering data decrease with increasing Q and, finally, the $S(Q)$ are dominated by noise. The Q_{max} used in the Fourier transforms (Eq. 1) were chosen accordingly with $400\,nm^{-1}$ (neutrons) and $250\,nm^{-1}$ (X-rays). Additionally, a damping factor $M(Q)$ according to Lorch was used for the X-ray data. This damping reduces those spurious ripples of the correlation functions that are due to the noise at large Q and the termination of the Fourier transform at Q_{max}. However, damping also causes an additional broadening of peaks, which could smear out interesting distance details such as the two P−O distances.

The correlation functions $T_N(r)$ (neutrons) and $T_X(r)$ (X-rays) were obtained as the Fourier transforms of the corresponding $S(Q)$ data with

$$T(r) = 4\pi\, r\rho_0 + \frac{2}{\pi}\int_0^{Q_{max}} Q\,[S(Q) - 1]\,M(Q)\sin(Qr)\,dQ \qquad (1)$$

The number densities of atoms, ρ_0, were calculated from the mass densities and glass compositions [7]. The $T_N(r)$ functions of the samples SNP50 and SNP55 did not oscillate around the zero line as expected for distances less than the shortest bond (P−O). That mismatch indicates normalization problems. These samples had the largest amounts of OH (1000–1600 ppm) [7] which could then cause an additional incoherent scattering that disturbs normalization. A small correction to the corresponding data was made.

Gaussian fitting of the first-neighbor peaks was performed by combination of both the $T_N(r)$ and $T_X(r)$ data. The effects of truncation at Q_{max}, damping and Q-dependent partial weighting factors were taken into account. Good agreement was obtained for distances < 0.27 nm for

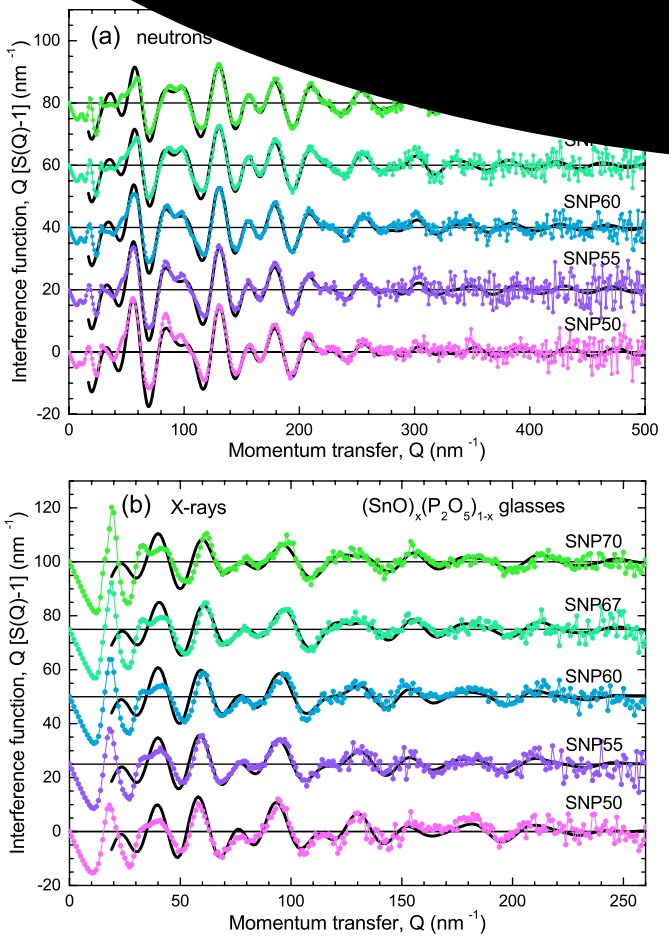

Fig. 1. Weighted interference functions, $Q{\cdot}[S(Q)\text{-}1]$: the experimental neutron (a) and X-ray (b) data of the five tin phosphate glasses studied (dotted lines) are compared with model functions (black solid lines) that are calculated by the parameters of the model first-neighbor peaks shown in Fig. 2. The upper curves are shifted for clarity.

$T_N(r)$ and < 0.24 for $T_X(r)$ (Fig. 2). The $T_x(r)$ functions shown in Fig. 2b were obtained without damping, and their agreement is good, as well, except of the P−O peaks of the SNP67 and SNP70 samples. The visible deficiencies are attributed to the normalization problems mentioned in Section 2.2. The $T_x(r)$ functions in Fig. 2b illustrate the compositional changes of the P−O, Sn−O and Sn−P peaks better than the others. The $T_N(r)$ were also calculated with $Q_{max} = 500\,nm^{-1}$ with damping according to Lorch and good agreement with the model peaks was found, as well. The resulting parameters of the Gaussian functions are given in Table A1 of Appendix A.

The neutron $T(r)$ functions show sharp peaks for the P−O and O−O first-neighbor distances at 0.15 and 0.25 nm, respectively, distances that describe a PO_4 tetrahedron. The P−O peak was decomposed with two Gaussian functions which take into account the different P−NBO (non-bridging oxygen) and P−BO (bridging oxygen) bond lengths. The ratio of peak areas was calculated according to the SnO content, and thus shows the expected degree of decomposition of the phosphate network with SnO additions. Below, we use the Q^n notation for different PO_4 groups (n is the number of P−O−P bridges on a tetrahedron) as it was introduced in structural studies by ^{31}P NMR spectroscopy [1,2,16,18,26]. The Q^n distributions change stepwise with binary Q^3 & Q^2, Q^2 & Q^1 to Q^1 & Q^0 populations as shown by ^{31}P NMR for the $(SnO)_x(P_2O_5)_{1-x}$ glasses [1,16]. The P−O peaks of the $T_N(r)$ functions show the change from Q^2 to Q^0 with increasing x. Two lengths of P−O bonds are obvious where the fraction of P−BO decreases. No P−BO bonds could be distinguished for the SNP70 sample. The subtle

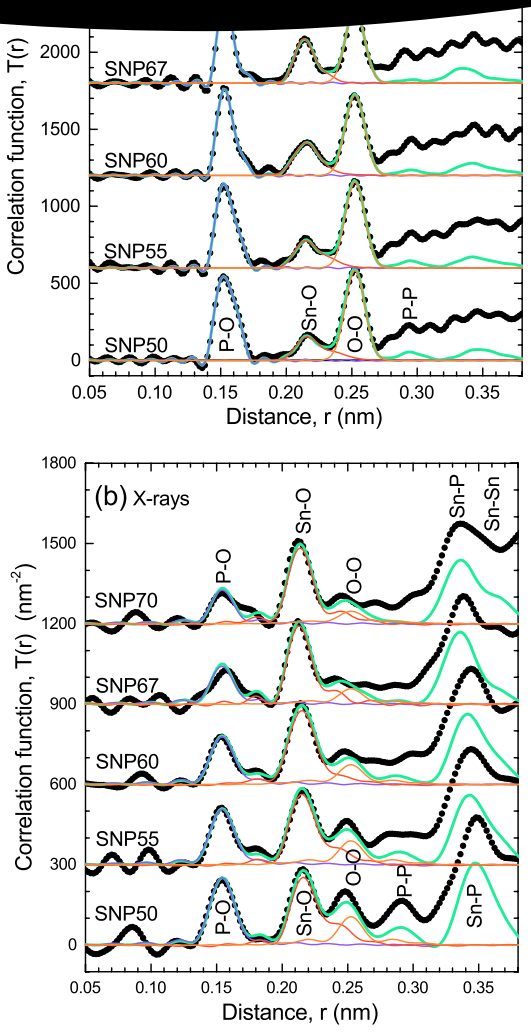

Fig. 2. Correlation functions $T(r)$ of the $(SnO)_x(P_2O_5)_{1-x}$ glasses obtained from neutron (a) and X-ray (b) $S(Q)$ functions from Fig. 1 with $Q_{max} = 400$ and $250\,nm^{-1}$ (no damping). The upper curves are shifted for clarity. The experimental curves (black dots) are compared with the model functions (thick cyan lines). The partial model peaks P-O, Sn-O and O-O are given with thin purple, red and orange lines, respectively. Note, the fits were made with other $T_X(r)$ functions that were obtained with Lorch damping. (For interpretation of the references to colour in this figure legend, the reader is referred to the web version of this article.)

lengthening of the P−NBO distances (cf. Table in Appendix A) reflects the decrease of bond strength in the change from Q^2 via Q^1 and Q^0 groups, whereas the mean length of P−O bonds is constant [27].

The Sn−O peaks are well resolved in the $T(r)$ functions. They are the dominant peaks in the $T_X(r)$, but are not fully separate from the O−O peak. The positions of the Sn−O maxima change very little with composition. The peak shapes are asymmetric with a tail to longer distances (smallest tail component for sample SNP67). The areas of the O−O peaks were calculated according to the number of PO_4 edges and the remaining distances in that range (0.25 nm) were attributed to the Sn−O component. (If the areas of O−O peaks were not fixed in this manner, one would obtain smaller O−O coordination numbers, N_{OO}, for the samples SNP50, SNP55 and SNP60, but even larger values of N_{SnO}.) The Sn−O distances were approximated by two or three Gaussian

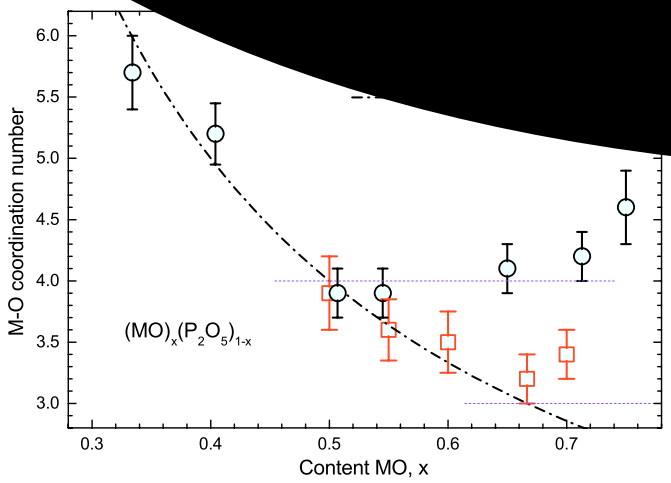

Fig. 3. Compositional behavior of the oxygen coordination numbers N_{MO} of Sn (red squares – this work) and Zn (black circles) of $(MO)_x(P_2O_5)_{1-x}$ glasses. The values N_{ZnO} are taken from [28–30]. The horizontal lines mark $N_{MO} = 3$ and 4. Value R_{NBO} is the ratio n(NBO)/n(M) [27,31]. (For interpretation of the references to colour in this figure legend, the reader is referred to the web version of this article.)

functions, and the corresponding parameters are given in Table A1 of Appendix A. Total coordination numbers and mean distances are also given. The compositional evolution of the values N_{SnO} is shown in Fig. 3 and compared with the N_{ZnO} from studies of $(ZnO)_x(P_2O_5)_{1-x}$ glasses [28–30]; the dash-dot line is a structural model [31], discussed below in Section 4. The values N_{SnO} include all oxygen neighbors of distances < 0.26 nm, and decrease from about four at 0.5 SnO to three at 0.67 SnO. At the same time, the Sn—P distances apparent in the $T_X(r)$ functions decrease from 0.345 to 0.335 nm with increasing SnO content.

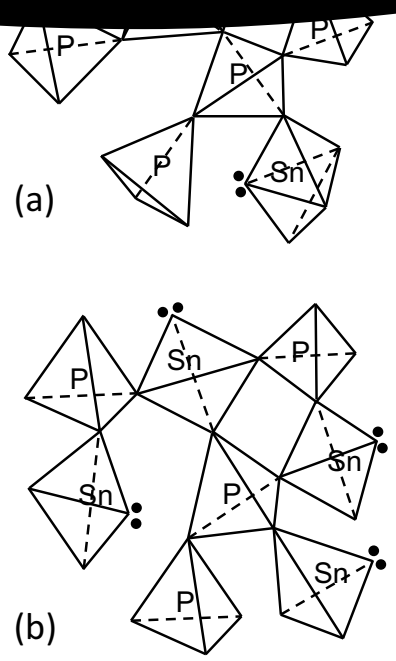

Fig. 4. Representative sections of the networks of Sn(II) phosphate glasses with SnO contents $x = 0.5$ (a) and 0.67 (b). All O atoms form either P–O–P or Sn–O–P bonds. The thick dots indicate those corners of SnO_4 or SnO_3 units with the lone-pair of non-bonding electrons. The central PO_4 and the upper SnO_z units of (a) and (b) show the respective number of PO_4 and SnO_z neighbors of that glass composition.

4. Discussion

It has been shown for a variety of different phosphate glasses that the coordination number of the metal modifying cation depends on the ratio between the number of non-bridging oxygens in the glass structure and the number of metal cations [27,31]. For the $(SnO)_x(P_2O_5)_{1-x}$ glasses, this ratio, $R_{NBO} = n$(NBO)/n(Sn) is given by

$$R_{NBO} = 2[1 + n(P_2O_5)/n(SnO)] = 2/x \quad (2)$$

For the compositional range $0.5 \le x \le 0.67$, R_{NBO} decreases from 4 to 3, corresponding to the replacement of SnO_4 units by SnO_3 units, as shown by the N_{SnO} data in Fig. 3. The implication of $R_{NBO} = N_{SnO}$ is that all NBO form P—O—Sn bridges and all SnO_z polyhedra are isolated by absence of Sn—O—Sn linkages. The crystal structure of $Sn_2P_2O_7$ [13] is similar, with the SnO_3 sites linking only pyrophosphate (P_2O_7) anions. Representative sections of the suggested glassy networks with SnO_4 trigonal bipyramids for $x = 0.5$ and SnO_3 trigonal pyramids for $x = 0.67$ are shown in Fig. 4. SnO_3 units are the only known example of three-coordinated modifier M^{2+} cations in phosphate glasses. The SnO_z polyhedra that constitute the crosslinked networks in Sn(II)-phosphate glasses have previously also been described as network forming sites [2].

When $x > 0.67$ and $R_{NBO} < 3$, there are insufficient NBOs to isolate all SnO_3 sites in the glass structure and so the Sn-polyhedra must share NBOs, forming Sn—NBO—Sn linkages. The shoulder on the right side of the Sn—P peak (Fig. 2b) indicates such Sn—Sn distances of 0.36 nm for sample SNP70. Another effect of this clustering is the small increase in N_{SnO}, from 3.2 to 3.3, when x increased from 0.67 to 0.70. From a bond valence perspective, larger SnO_x polyhedra will contribute less valence charge per oxygen bond and so a cluster of larger polyhedra will not overcharge the non-bridging oxygen to the extent that smaller polyhedra will.

Further support for the change of N_{SnO} and the networks suggested in Fig. 4 comes from the observed peak widths of the Sn—O distances and the change of Sn—P distances. The most narrow Sn—O peak is found for sample SNP67 when compared with the other glasses. Here, the SnO_3 units with three equivalent bond lengths dominate and they are not affected by sharing NBOs in Sn—NBO—Sn linkages such as for sample SNP70. A considerable fraction of the Sn—O bonds of the samples SNP50 and SNP55 are clearly longer than 0.213 nm, which is characteristic for the SnO_4 bipyramids with two different bond lengths. Accordingly, their Sn—P distances must also be longer than those of a network with only SnO_3 units. As expected, the Sn—P distances decrease from 0.345 nm (SNP50) to 0.335 nm (SNP67) (cf. Fig. 2b).

Another change in N_{SnO} was noted in a recent diffraction study of $(ZnO)_y(SnO)_{0.67-y}(P_2O_5)_{0.33}$ glasses, where N_{SnO} increased from three to four with y increasing from 0.0 to 0.40 [18]. Thus, the ZnO_4 units do not simply replace the SnO_3 (structure shown in Fig. 4b) but they force the remaining SnO_3 to change to SnO_4. Isolated ZnO_4 sites required more NBOs than were available at the pyrophosphate composition. Those tetrahedra likely were incorporated in clusters with SnO_4 polyhedra, again to reduce the valence charge on the common NBO. The resulting compaction of the structure produced an increase in the mass density of these glasses with increasing values of y [32] even though Zn is lighter than Sn by a factor 0.55. Part of the structural compaction could also be due to smaller ZnO_4 tetrahedra replacing the SnO_3 or SnO_4 pyramids, a consequence of the steric contributions of the lone-pair associated with the apex of these SnO_z pyramids.

The structural characteristics of the SnO_z and PO_4 units that form the continuous networks in the compositional range $0.5 \le x \le 0.67$

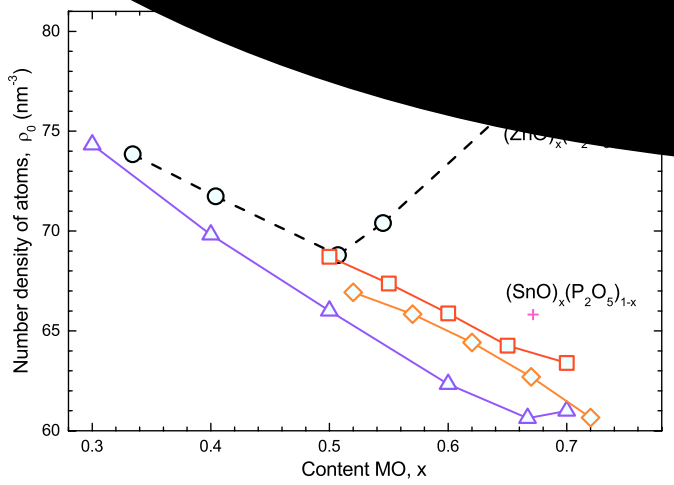

Fig. 5. Compositional evolution of the number densities of atoms, ρ_0, of $(MO)_x(P_2O_5)_{1-x}$ glasses: for M = Sn (red squares – this work and [7], orange diamonds – [5], purple triangles – [1] pycnometer densities); for M = Zn (black circles – [28,29]). The plus sign (red) indicates the density of the $Sn_2P_2O_7$ crystal [13]. (For interpretation of the references to colour in this figure legend, the reader is referred to the web version of this article.)

produce a decrease of ion packing density with increasing values of x (open squares in Fig. 5). Here, the number densities of atoms, ρ_0, were calculated from the mass densities and sample compositions and so avoid the influence of the large atomic mass of Sn when considering the compositional dependence of the glass structure. The change from SnO_4 to SnO_3 units (cf. Fig. 3) with increasing x is accompanied by a continuous decrease in ρ_0 (Fig. 5). The number densities of atoms in $(SnO)_x(P_2O_5)_{1-x}$ glasses from two other studies are also shown [1,5] and give similar trends. The density of the only known related crystal [13] (65.9 nm^{-3}) is found just above the corresponding glass values.

Coordination number and Zn—O bond lengths in binary $(ZnO)_x(P_2O_5)_{1-x}$ glasses are somewhat similar to those of the Sn(II) phosphate glasses. However, the different behavior for $0.5 \le x \le 0.67$ with constant $N_{ZnO} = 4$ and the transition SnO_4 to SnO_3 cause different trends of properties. The corresponding number densities of atoms of the $(ZnO)_x(P_2O_5)_{1-x}$ glasses are compared in Fig. 5. The values of ρ_0 for the Zn-ultraphosphate glasses ($x < 0.5$) decrease with increasing values of x, but then clearly increase for $x > 0.5$. At $x = 0.5$, $R_{NBO} = 4$ and this glass will form a continuous network with isolated ZnO_4 tetrahedra linking the metaphosphate anions through Zn—O—P bonds, as seen, for example in the structure of crystalline β-$Zn(PO_3)_2$ [33]. This behavior is similar with that in the glass SNP50 with SnO_4 pyramids. When $x > 0.5$, $R_{NBO} < 4$ and so there are insufficient NBOs to accommodate all Zn^{2+} ions in isolated tetrahedral sites. As a consequence, Zn—O polyhedra must share NBOs. A fraction of three-coordinated NBOs develops and its amount increases with x with the formation of a Zn—O—Zn subnetwork.

To explain the number density of atoms in relation to the oxygen coordination number N_{MO} (M = Sn,Zn) it is assumed that a high average number (N_{av}) of neighboring groups linked to a polyhedron (PO_4 and MO_z) is the critical value that determines a compact structure. Those neighboring groups are counted which share common oxygen neighbors with a given central group. The detailed effects of different bond lengths, e.g., PO_4 with short P—O—P bonds will form more compact structures than the MO_z polyhedra with longer M—O—P and M—O—M bonds, are neglected here. Table 1 shows the values of N_{MM}, N_{MP}, and N_{PP}, obtained from simply counting the links associated with various groups, for three different glass compositions, and N_{av} is calculated from the corresponding numbers. If $N_{MO} = R_{NBO}$, then N_{av} decreases continuously with increasing x and the corresponding number density ρ_0 also decreases. That was found for M = Sn (cf. Fig. 5) and

MO content x	n(M)/n(P)	R_{NBO}	N_{MO}	N_{MM}	N_{MP}	N_{PM}	N_{PP}	N_{av}	M
0.33	1:4	6.0	6.0	0	6.0	1.5	2.5	4.4	Zn
0.50	1:2	4.0	4.0	0	4.0	2.0	2.0	4.0	Zn, Sn
0.67	1:1	3.0	3.0	0	3.0	3.0	1.0	3.5	Sn
0.67	1:1	3.0	4.0	2.0	4.0	4.0	1.0	5.5	Zn

also for M = Zn with $x \le 0.5$. For $x > 0.5$, the ZnO_4 units must share NBOs and this means that the values of N_{ZnZn}, N_{ZnP}, and N_{PZn} for $x = 0.67$ are larger than the corresponding numbers for the tin phosphate glass, leading to N_{av} values of 5.5 (ZnO) and 3.5 (SnO), respectively, accounting for the greater number densities of atoms in the Zn glasses (Fig. 5). The N_{ZnZn}, N_{ZnP}, and N_{PP} values of a zinc phosphate glass of $x = 0.64$, obtained by structural modelling (Reverse Monte Carlo) [34], produce an N_{av} value of 5.6, similar to the value of 5.5 in Table 1.

Finally, we consider the structures of Sn(II)-phosphate glasses in the compositional range $x < 0.5$, the ultraphosphate range. Like the Zn-ultraphosphate glasses, the number densities (ρ_0) reported in the literature [1,16] for the Sn(II)-ultraphosphate glasses increase systematically as x decreases in the range $x < 0.5$. Diffraction studies of the Zn-ultraphosphate glasses have shown that the average N_{ZnO} increases in this same range, following the predictions of the R_{NBO} values (Fig. 3), and it seems reasonable that similar trends will exist for the Sn(II)-ultraphosphate glasses. The authors of ^{119}Sn Mössbauer [8] and ^{119}Sn NMR [16] spectroscopic studies report changes in the respective spectral parameters for glasses in the ultraphosphate range, and attributed these changes to distortions by additional oxygens on more distant positions than typical for single bonds. The presence of such SnO_{4+1} or SnO_{3+2} units are consistent with the R_{NBO} structural model.

Analogs for the distorted Sn-polyhedra predicted for the Sn-ultraphosphate glasses may be found in diffraction studies of $(TeO_2)_x(P_2O_5)_{1-x}$ glasses [35]. Although Te^{4+} has a larger charge, its size and the lone-pair are features similar to those of Sn(II). The coordination numbers N_{TeO} follow approximately the predictions of the ratio R_{NBO}, including the formation of TeO_{4+1} or TeO_5 units. (The 4 + 1 means that one Te—O bond is longer (by ~0.04 nm) than the other four). Quantitative analysis of the diffraction data was difficult due to the formation of distorted TeO_z units. The Te—O correlations do not show narrow first-neighbor peaks but rather broad and asymmetric peak shapes. An advantage of the Te phosphate system was the knowledge of related crystal structures [36,37] that provided examples of TeO_{4+1} or TeO_5 units. Due to the smaller charge of Sn^{2+}, the distortions may be even stronger and a determination of SnO_5 units will be difficult. XRD by high-energy photons rather than neutron diffraction or both methods are needed. Unfortunately, Sn is not optimal for image plate technique in XRD, as outlined above.

5. Conclusions

The neutron diffraction results for the $(SnO)_x(P_2O_5)_{1-x}$ glasses studied ($0.5 \le x \le 0.7$) show the expected changes in the P—O peak, reflecting an increase in the fraction of P—NBO bonds with SnO additions. The Sn—O coordination number decreases from four at metaphosphate composition ($x = 0.5$) to about three at the pyrophosphate composition ($x = 0.67$). The structural units are assumed, respectively, to be SnO_4 trigonal bipyramids and SnO_3 trigonal pyramids with the lone-pair of the Sn(II) in one of the polyhedral corners, as is known for the related crystal structures. The observed peak widths of the Sn—O distances and the changes in the Sn—P distances are consistent with the systematic

decrease in N_{SnO} w

For all glasses up to
change in agreement with the ava
the Sn^{2+} ions. Thus, the PO_4 tetrahedra
with only P—O—P and P—O—Sn bridges with isolated
The Sn^{2+} ions do not share oxygen neighbors in this compositional range, but do form such clusters when x > 0.67.

The different trends for the number densities of atoms of the Sn and Zn phosphate glasses of similar compositions (0.5 < x < 0.67) confirm the different respective behavior of N_{SnO} and N_{ZnO} values. The ZnO_4 tetrahedra share NBOs in this compositional range, causing an increase in atom number density, whereas the continuous conversion of SnO_4 to SnO_3 in this compositional range decreases atom number density. The atom number densities of the Sn and Zn ultraphosphate glasses ($x < 0.5$) follow similar compositional trends, and since

environments of Te(IV)-phosphate glasses, another cation environment distorted by lone-pair electrons.

Acknowledgements

The Sn-phosphate glasses were prepared by Jong-Wook Lim for his Masters' degree thesis at the Missouri University of Science and Technology.

Appendix A. Appendix

Table A1
Parameters of the Gaussian functions used for fitting the first-neighbor peaks of the X-ray and neutron $T(r)$ functions. The values marked with asterisks were fixed in the fits. Parameters of the single Gaussian peaks are not given with uncertainties because the ratio P-NBO/P-BO was fixed. The areas of the two or three Gaussians of the Sn-O bonds are not free of arbitrariness because these components are broad and overlap.

Sample label	Atom pair	Coord. number	Distance (nm)	fwhm (nm)	Total coord. number	Mean distance (nm)
SNP50	P—NBO	1.95	0.1495	0.009	3.95 ± 0.15	0.1548 ± 0.0015
	P—BO	2.00	0.160	0.011		
	Sn—O	2.6	0.2155	0.019	3.9 ± 0.3	0.223 ± 0.002
		0.9	0.235	0.022		
		0.4	0.250	0.026		
	O—O	4.00*	0.2525*	0.0175		
SNP55	P—O	2.30	0.1507	0.010	3.85 ± 0.15	0.1550 ± 0.0015
		1.55	0.1613	0.011		
	Sn—O	2.6	0.2142	0.019	3.7 ± 0.3	0.221 ± 0.002
		0.8	0.232	0.022		
		0.3	0.250	0.026		
	O—O	3.86*	0.2525*	0.0173		
SNP60	P—O	2.45	0.1515	0.010	3.90 ± 0.15	0.155 ± 0.0015
		1.45	0.1612	0.013		
	Sn—O	2.8	0.214	0.0205	3.5 ± 0.2	0.218 ± 0.002
		0.6	0.228	0.022		
		0.1	0.250	0.026		
	O—O	3.7*	0.2525*	0.0175		
SNP67	P—O	2.95	0.1525	0.010	3.95 ± 0.15	0.1549 ± 0.0015
		1.00	0.162	0.013		
	Sn—O	2.65	0.213	0.016	3.2 ± 0.2	0.216 ± 0.002
		0.55	0.2285	0.018		
	O—O	3.43*	0.2525*	0.0163		
SNP70	P—O	3.15	0.1532	0.010	3.90 ± 0.15	0.1548 ± 0.0015
		0.75	0.1617	0.012		
	Sn—O	2.8	0.2135	0.019	3.3 ± 0.2	0.217 ± 0.002
		0.3	0.232	0.022		
		0.2	0.250	0.026		
	O—O	3.30*	0.2525*	0.018		

References

[1] D. Holland, A.P. Howes, M.E. Smith, A.C. Hannon, Lone-pair effects and structural trends in xSnO·(1-x) P_2O_5 glasses deduced from ^{31}P and ^{119}Sn nuclear magnetic resonance, J. Phys. Condens. Matter 14 (2002) 13609–13621.

[2] E. Bekaert, L. Montagne, L. Delevoye, G. Palavit, A. Wattiaux, NMR and Mössbauer characterization of tin(II)-tin(IV)-sodium phosphate glasses, J. Non-Cryst. Solids 345&346 (2003) 70–74.

[3] M. Guignard, L. Albrecht, J.W. Zwanziger, Zero-stress optic glass without lead, Chem. Mater. 19 (2007) 286–290.

[4] H. Takebe, W. Nonaka, T. Kubo, J. Cha, M. Kuwabara, Preparation and properties of transparent SnO-P_2O_5 glasses, J. Phys. Chem. Solids 68 (2007) 983–986.

[5] J. Cha, T. Kubo, H. Takebe, M. Kuwabara, Compositional dependence of properties of SnO-P_2O_5 glasses, J. Ceram. Soc. Jpn. 116 (2008) 915–919.

[6] J.W. Lim, M.L. Schmitt, S.W. Yung, R.K. Brow, Properties and structures of tin borophosphate glasses, J. Non-Cryst. Solids 356 (2010) 1379–1384.

[7] J.W. Lim, S.W. Yung, R.K. Brow, Properties and structure of binary tin phosphate glasses, J. Non-Cryst. Solids 357 (2011) 2690–2694.

[8] V. Martin, U. Werner-Zwanziger, J.W. Zwanziger, R.A. Dunlap, Correlation of structure and photoelastic response in tin phosphate glass, Int. J. Appl. Glas. Sci. 2 (2011) 282–289.

[9] H. Masai, T. Yanagida, Y. Fujimoto, M. Koshimizu, T. Yoko, Scintillation property of rare earth-free SnO-doped oxide glass, Appl. Phys. Lett. 101 (2012) 191906.

[10] N. Yamamoto, A. Saitoh, H. Takebe, Zero photoelastic zinc tin phosphate glass without lead oxide, Opt. Lett. 37 (2012) 4203–4205.

[11] K.H. Jost, Die Struktur des Bleipolyphosphats $[Pb(PO_3)_2]_x$ und allgemeiner Überblick über Polyphosphatstrukturen, Acta Crystallogr. 17 (1964) 1539–1544.

[12] U. Hoppe, G. Walter, D. Stachel, A.C. Hannon, Short-range order details of meta-phosphate glasses studied by pulsed neutron scattering, Z. Naturforsch. 50a (1995) 684–692.

[13] V.V. Chernaya, A.S. Mitiaev, P.S. Chizhov, E.V. Dikarev, R.V. Shpanchenko, E.V. Antipov, M.V. Korolenko, P.B. Fabritchnyi, Synthesis and investigation of tin (II) pyrophosphate $Sn_2P_2O_7$, Chem. Mater. 17 (2005) 284–290.

[14] W. Shengfeng, C. Kueibo, L. Chishen, Synthesis and characterization of alkali-metal tin(II) phosphates: $Na_{10}Sn_{31}(HPO_4)_6(P_2O_7)_6(PO_4)_{12}$ and $K_2Sn(P_2O_7)$, Solid State Sci. 10 (2008) 1485–1490.

[15] J.F. Bent, A.C. Hannon, D. Holland, M.M.A. Karim, The structure of tin silicate glasses, J. Non-Cryst. Solids 232-234 (1998) 300–308.

[16] Y. Xia, M.A.T. Marple, I. Hung, Zh. Gan, S. Sen, Network structure and connectivity

in $SnO\text{-}P_2O_5$ glass
Chem. B 122 (2018) 74
[17] K.E. Kweon, V. Lordi, First prin
properties of Sn^{2+}-doped $ZnO\text{-}P_2O_5$ gla
108–114.
[18] U. Hoppe, A. Saitoh, G. Tricot, P. Freudenberger, A.C. Hannon,
R.K. Brow, The structure and properties of xZnO-(67-x)SnO-$33P_2O_5$ glasses: (I)
diffraction, NMR, and chromatographic studies, J. Non-Cryst. Solids 492 (2018)
68–76.
[19] D. Waasmaier, A. Kirfel, New analytical scattering-factor functions for free atoms
and ions, Acta Crystallogr. A51 (1995) 416–431.
[20] E.N. Maslen, A.G. Fox, M.A. O'Kiefe, in: A.J.C. Wilson (Ed.), *International Tables for Crystallography*, Vol. C, Kluwer Academic, Dordrecht, 1992, p. 476.
[21] J.H. Hubbell, Wm.J. Veigele, E.A. Briggs, R.T. Brown, D.T. Cromer, R.J. Howerton,
Atomic form factors, incoherent scattering functions, and photon scattering cross
sections, J. Phys. Chem. Ref. Data 4 (1975) 471–538.
[22] T.E. Faber, J.M. Ziman, A theory of the electrical properties of liquid metals, Philos.
Mag. 11 (1965) 153–173.
[23] Y. Waseda, The Structure of Non-Crystalline Materials, McGraw-Hill, New York,
1980, p. 11.
[24] U. Hoppe, L. Delevoye, L. Montagne, M.v. Zimmermann, A.C. Hannon, Structure of
Nb_2O_5-$NaPO_3$ glasses by X-ray and neutron diffraction, Phys. Chem. Chem. Phys. 15
(2013) 8520–8528.
[25] A.C. Hannon, Results on disordered materials from the general materials diffractometer, GEM, at ISIS, Nucl. Instr. Meth. A 551 (2005) 88–107.
[26] R.K. Brow, Review: the structure of simple phosphate glasses, J. Non-Cryst. Solids
263 & 264 (2000) 1–28.
[27] U. Hoppe, G. Walter, R. Kranold, D. Stachel, Structural specifics of phosphate
glasses probed by diffraction methods: a review, J. Non-Cryst. Solids 263 & 264
[30] U. Hoppe, I. Dimitrov, J. Neuefeind, Structure of zinc phosphate glasses of 75 and 80
mole% ZnO content studied by X-ray diffraction and reverse Monte Carlo simulations, Z. Naturforsch. 60a (2005) 517–526.
[31] U. Hoppe, A structural model for phosphate glasses, J. Non-Cryst. Solids 195 (1995)
138–147.
[32] A. Saitoh, R.K. Brow, U. Hoppe, G. Tricot, S. Anan, H. Takebe, The structure and
properties of x(ZnO)-(67-x)SnO-$33P_2O_5$: (I) optical and thermal properties, Raman
and infrared spectroscopies, J. Non-Cryst. Solids 484 (2018) 132–138.
[33] M. Weil, The high-temperature modification of zinc catena-polyphosphate, β-Zn
$(PO_3)_2$, Acta Crystallogr. C60 (2004) i20–i22.
[34] U. Hoppe, G. Walter, G. Carl, J. Neuefeind, A.C. Hannon, Structure of zinc phosphate glasses probed by neutron and X-ray diffraction of high resolving power and
by reverse Monte Carlo simulations, J. Non-Cryst. Solids 351 (2005) 1020–1031.
[35] U. Hoppe, I. Gugov, H. Bürger, P. Jóvári, A.C. Hannon, Structure of tellurite glasses
– effects of K_2O or P_2O_5 additions studied by diffraction, J. Phys. Condens. Matter
17 (2005) 2365–2386.
[36] H. Mayer, M. Weil, Synthese und Kristallstruktur von $Te_3O_3(PO_4)_2$ – eine
Verbindung mit fünffach koordiniertem Tellur(IV), Z. Allg. U. Anorg. Chemie 629
(2003) 1068–1072.
[37] M.K. Kim, S.-H. Kim, H.-Y. Chang, P.S. Halasyamani, K.M. Ok, New non-
centrosymmetric tellurite phosphate material: synthesis, characterization, and calculations of $Te_2O(PO_4)_2$, Inorg. Chem. 49 (2010) 7028–7034.